Reprinted from



REGULAR PAPER

First Principles Calculations of Linear and Second-Order Optical Responses in Rhombohedrally Distorted Perovskite Ternary Halides, $CsGeX_3$ (X = Cl, Br, and I)

Li-Chuan Tang, Yia-Chung Chang, Jung-Yau Huang, Ming-Hsien Lee, and Chen-Shiung Chang Jpn. J. Appl. Phys. **48** (2009) 112402

First Principles Calculations of Linear and Second-Order Optical Responses in Rhombohedrally Distorted Perovskite Ternary Halides, $CsGeX_3$ (X = Cl, Br, and I)

Li-Chuan Tang¹, Yia-Chung Chang^{1,2}, Jung-Yau Huang¹, Ming-Hsien Lee³, and Chen-Shiung Chang^{1*}

Received March 24, 2009; revised July 28, 2009; accepted July 29, 2009; published online November 20, 2009

Systematic studies based on first-principles calculations of second-order optical susceptibilities as well as the dielectric function of CsGeX₃ (X = CI, Br, and I; CGX) are presented. The relationship between structural properties and optoelectronic responses are examined. The structural factors $\Delta \alpha$, and d_{Ge} , d_{X} are proposed to describe the degree of distortion from an ideal perovskite structure. $\Delta \alpha$ and d_{Ge} increase when halide anions are changed from CI to I; while halide anion displacement, d_{X} , decreases. The structural distortion effect on these rhombohedral CGX crystals is analyzed by first-principles calculations. The dielectric function and the second harmonic generation (SHG) response coefficient also increase with increasing $\Delta \alpha$ and d_{Ge} . The direct band gaps (E_{G}) of CsGeX₃ all occur at the R-point, ΔE_{R} . The experimental band gaps of CGX crystals become smaller, i.e., $E_{\text{G}}^{\text{CGC}}$ (= 3.67 eV) > $E_{\text{G}}^{\text{CGB}}$ (= 2.32 eV) > $E_{\text{G}}^{\text{CGI}}$ (= 1.53 eV), as $\Delta \alpha$ and d_{Ge} increase, i.e., $d_{\text{Ge}}^{\text{CGS}}$ < $d_{\text{Ge}}^{\text{CGI}}$ < $d_{\text{Ge}}^{\text{CGI}}$. Partial density of states (PDOS) analysis revealed that the valence band maximum (VBM) and conduction band minimum (CBM) are mainly contributed by the p-orbitals of germanium. The calculated magnitudes of $\chi_{ijk}^{(2)}$ are close to some reported experimental values near the band gap. © 2009 The Japan Society of Applied Physics

DOI: 10.1143/JJAP.48.112402

1. Introduction

Second-order nonlinear optical (NLO) materials have played a key role in various areas of optics, such as laser frequency conversion and optical parametric oscillation/amplification (OPO/OPA).^{1,2)} Recently, several ternary halides in ABX₃ $(A = Cs, Rb, B = Ge, Cd, X = Cl, Br, I)^{3-10}$ have been discovered to exhibit second-order NLO properties. Rhombohedral CsGeCl₃ (CGC) was found to possess excellent second-order NLO properties, displaying a second-harmonic generation (SHG) efficiency 5 times larger than that of KH₂PO₄ (KDP) and a damage threshold of 200 MW/cm^{2.8)} The electronic and linear optical properties of CsGeI₃ (CGI) were also reported by Tang et al.⁶⁾ At the same time, CsCdBr₃ was found by Ren et al.¹¹⁾ to be noncentrosymmetric (NCS), i.e., the symmetry of the inversion center is absent. Rhombohedral CsGeBr₃ (CGB), which was found to possess better second-order NLO properties than CGC, exhibits a SHG efficiency of 10 times larger than KDP. 10) The ternary halides have recently become a new category of nonlinear optical (NLO) materials, which are potentially applicable from the visible to infrared regions.

To apply this new category of NLO crystals to infrared SHG materials, the following attributes need to be considered: transparency in the relevant wavelengths, ability to withstand laser irradiation, and chemical stability. Most importantly, the material in question must be crystallographically NCS. Mathematically, it has been known for some time that only an NCS arrangement of atoms may produce a second-order NLO response. ^{12–14)}

In this paper, rhombohedral CsGeX₃ (CGX, X = Cl, Br, I) crystals are focused on. These CGX crystals have certain interesting properties. First of all, all CGX materials have a similar crystal sructure, and they possess identical space group symmetry, i.e., R3m (160). The conventional empirical equation, that is, the Goldschmidts tolerence factor, ^{15,16} cannot accurately predict their crystal structures. A CGX crystal is rhombohedrally deformed from an ideal perovskite

crystal structure. Second, they all have very large NLO susceptibility. Third, the transparent spectrum of CGX can be extended to a very long wavelength ($\geq 20\,\mu m$) in the infrared region. Therefore, CGX can be applied to wider-optical-spectrum investigations. The only shortcoming for CGX crystals is that their size and quality need to be improved. In this study, the first two properties mentioned above would be emphasized. To understand these properties, systematrical analysis of the effect of the structural factor of CGS crystals on their electronic and optical properies would be carried out. Both the experimental and calculated lattice parameters will be compared in §2.

The analytic expressions of the nonlinear response functions are based on the formalism of Sipe and Ghahramani, ¹⁷⁾ as extended and developed in length gauge by Aversa and Sipe; ¹⁸⁾ the response calculation is at the level of independent particle approximation. This approach has the advantage that response coefficients are inherently free of any nonphysical divergences at zero frequency, a consequence of a careful treatment and separation of interband and intraband transitions. "Sum rules" are not required to eliminate artificial divergences. The recent work of Dal Corso and Mauri, ¹⁹⁾ based on an elegant Wannier function approach, is also free of such divergences.

The full-band structure calculation in this work utilized the norm-conserving pseudo potential plane wave (ppp) within local density approximation (LDA). This first-principles method is more reliable than the empirical method employed by Moss and co-workers. ^{20–24} Huang and Ching ^{25–27} neglect the "scissors" modification in matrix elements; based on evidence, ²⁸ and the results of our own calculations, this does not affect much the tendency in the determination of response functions. Local field effects were not included in this work. As suggested by the work of Levine and Allan, ²⁸ significant corrections for the materials considered here at the level of second-order response are expected. However, the inclusion of local field effects can be done in a straightforward manner within our formalism.

The paper is organized as follows. In §2 the distorted structure factors and their implementation are described, and

¹ Department of Photonics and Institute of Electro-Optical Engineering, National Chiao Tung University, Hsinchu 30010, Taiwan, R.O.C.

²Research Center for Applied Science, Academia Sinica, Taipei 11529, Taiwan, R.O.C.

³ Department of Physics, Tamkang University, Taipei 25137, Taiwan, R.O.C.

	а	α	a_{Ge}		$X_{a,b,c}$		$t_{ m G}$
CGC_{exp}	5.4342	89.723	0.4810	0.502400	0.502400	0.053800	1.0272
CGB_{exp}	5.6359	88.744	0.4764	0.501800	0.501800	0.027100	1.0094
CGI_{exp}	5.9830	88.600	0.4703	0.502900	0.502900	0.011900	0.9846
CGC_{calc}	5.5108	89.121	0.4799	0.502848	0.502848	0.058529	
CGB_{calc}	5.6885	88.297	0.4709	0.502245	0.502245	0.031737	
CGI_{calc}	5.9984	87.655	0.4646	0.506888	0.506888	0.010163	

Table I. Lattice constants and Ge and the X fractional coordinates of the rhombohedral NLO crystals CsGeX₃.

the analytic expressions or the linear and nonlinear response functions are presented. The band structures of the materials considered are also presented. The linear combination atomic orbital (LCAO) method and the calculation procedures used in determining the linear response and linear electro-optic (LEO) function are outlined and discussed in §3. In §4, we present the results for NLO coefficients. The comparison of our theoretical calculations with experiment and other theoretical calculations is discussed. A conclusion of our results is presented in §5.

2. Structural Factors and First-Principles Calculation

In an ideal perovskite structure, the cell parameters are a=b=c and $\alpha=\beta=\gamma=90^\circ$ with the cubic space group $Pm\bar{3}m$ (No. 221). Examples are the higher-temperature phase of cubic CsGeCl₃ and CsGeBr₃. ^{29–33}) The cell parameters of cubic CsGeBr₃ are $a=b=c=5.362\,\text{Å}$ and $\alpha=\beta=\gamma=90^\circ$ with the space group $Pm\bar{3}m$ (No. 221). The cell edges of rhombohedral (room-temperature phase) CsGeBr₃ are longer than those of the cubic (higher-temperature) phase, and the cell angles of rhombohedral (room-temperature phase) CsGeBr₃ become slightly smaller than 90° .

2.1 Structural factors

Structural distortion is considered as one of the dominant contributions of CsGeX₃ optical nonlinearity. With perovskite-type ternary oxides ABO₃ as well as halides CsGeX₃, Goldschmidt's tolerance factor $t_{\rm G}^{15,16}$ serves as a discriminating parameter for classifying perovskites in terms of structure modifications and the resulting physical properties.^{34–38)} The type of stacking depends on the tolerance factor $t_{\rm G}^{15,16}$

$$t_{\rm G} = \frac{r_{\rm A} + r_{\rm X}}{\sqrt{2} \cdot (r_{\rm B} + r_{\rm X})},\tag{1}$$

where A denotes a large cation, B a smaller cation, X an anion, and r the ionic radii of Shannon and Prewitt, ^{39,40)} which depend on the coordination number and bonding species. According to the emperical condition, a crystal structure can approach an ideal perovskite model when $0.97 \le t_G \le 1.03$. The structural parameters of CsGeBr₃, which were previously reported by JCPDS, ^{29–33)} are listed in Table I, for comparison. Accordingly the reported lattice room-temperature parameters of CsGeX₃ are listed in Table I, and the calculated atomic positions of ternary halide crystals are summarized in the last three rows for comparison. The tolerance factors, t_G , of the CsGeX₃ crystal structure are 1.009(4), 1.027, and 0.984. (see the far right

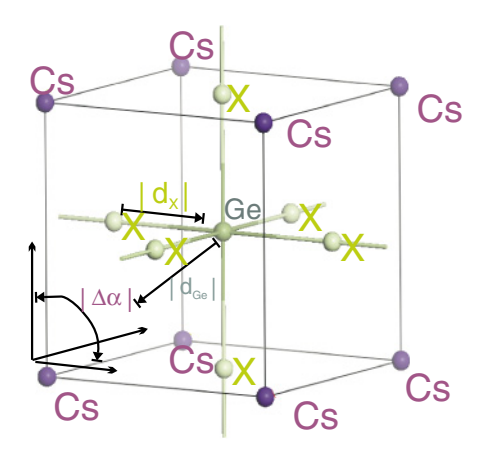


Fig. 1. (Color online) Crystal structure of rhombohedral $CsGeX_3$ is distorted from an ideal perovskite structure. The labels in the figure are the names of species (X = Cl, Br, and I) and the proposed rhombohedral distortion factors.

column in Table I). They are close to that of the empirically ideal perovskite structure ($t_G = 1.0$). CGX should behave like an ideal perovskite structure. However, CsGeX₃ crystals are all distorted to have a rhombohedral structure. Some extra structure factors are considered in this paper to deduce a better description.

We define the deviation of lattice angle from the ideal perovskite structure as

$$\Delta \alpha = \frac{90 - \alpha_{\text{rhomb}}}{90} \times 100, \tag{2}$$

the B-site cation, (i.e., germanium), displacement along the diagonal axis from the cell center to a corner as

$$d_{\text{Ge}}^{\text{rhomb}} = |(\mathbf{r}_{\text{Ge}}^{\text{fc}} - \mathbf{r}_{\text{Ge}}^{\text{rhomb}})| \times 100, \tag{3}$$

and the anion displacement (for Cl, Br, and I) as

$$d_{\mathbf{X}}^{\text{rhomb}} = |(\mathbf{r}_{\mathbf{X}}^{\text{fc}} - \mathbf{r}_{\mathbf{X}}^{\text{rhomb}})| \times 100, \tag{4}$$

where r is the position vector of ions in units of lattice constants. These factors are also indicated in Fig. 1. The structural distortion factors obtained from experimental and the first-principles calculation are listed in Table II. As shown in Table II, $\Delta \alpha$ and $d_{\rm Ge}$ become larger while $d_{\rm X}$ and $t_{\rm G}$ become smaller as atomic weight increases.

2.2 First-principles calculations

First-principles calculations are performed on the basis of the plane-wave-pseudopotential approach within the framework of density-functional theory (DFT) implemented in the CASTEP package.⁴¹⁾ To save computation time, eight k

Table II. Distorted structural factors are obtaind from the experimental and the first-principles calculated lattice constants of the rhombohedral NLO crystals $CsGeX_3$.

	$\Delta \alpha$	d_{Ge}	d_{X}
CGC_{exp}	3.078	1.90	5.391
CGB_{exp}	13.955	2.36	2.722
CGI_{exp}	15.555	2.97	1.259
CGC_{calc}	9.767	2.01	5.867
CGB_{calc}	18.922	3.00	3.189
CGI_{calc}	26.055	3.54	1.408

points $(3 \times 3 \times 3 \text{ mesh})$ are used for the calculation of the equilibrium lattice constants and mechanical properties. The geometrically optimized cell parameters and distortion factors are listed below the experimental results in Tables I and II, respectively. Similarly to the experimental results, the calculated $\Delta\alpha$ and $d_{\rm Ge}$ become larger, while dX becomes smaller as atomic weight increases, i.e., $\Delta\alpha^{\rm CGC} < \Delta\alpha^{\rm CGB} < \Delta\alpha^{\rm CGG}$ and $d_{\rm Ge}^{\rm CGG} < d_{\rm Ge}^{\rm CGB} < d_{\rm Ge}^{\rm CGI}$.

The summation over the Brillouin zone (BZ) is carried out

The summation over the Brillouin zone (BZ) is carried out with a special k-point sampling using the $54 \times 54 \times 54$ Monkhorst–Pack grid⁴²⁾ in the calculation of optical properties. A kinetic-energy cutoff of 500 eV and 51 bands are used to ensure the convergence.

2.2.1 Electronic properties

The lattice parameters obtained above are used in the calculation of the electronic properties of $CsGeX_3$. To understand the nature of optical transitions and other relevant effects on the calculated optical properties, an analysis of the local densities of states and other electronic properties of these $CsGeX_3$ crystals is carried out.

2.2.2 Linear combination of atomic orbital method

To determine the optical response functions in the full-band structure approach, one requires eigenvalues and velocity matrix elements at many ${\bf k}$ points in BZ. The velocity matrix elements, in turn, require a knowledge of electronic wave functions. For this purpose, we employ a first-principles approach in the form of LCAO method. As this method was previously discussed, ^{43,44)} we highlight only a few of its pertinent features.

Let $\Psi_{nk}(\mathbf{r})$ be the self-consistent wave function of the crystal at the *n*-th band and *k*-th point in BZ. $\Psi_{nk}(\mathbf{r})$ can be decomposed into a linear combination of the atomic orbitals $\Phi_{lm}^{(i)}(\mathbf{r})$ of *i*-th atom by

$$\Psi_{nk}(\mathbf{r}) = \sum_{i \in (\text{atoms})} \sum_{l} \sum_{m=-l}^{m=+l} C_{nk,lm}^{(i)} \Phi_{lm}^{(i)}(\mathbf{r}),$$
 (5)

where $C_{nk,lm}^{(i)} = \int_{V_0} \Psi_{nk}(\mathbf{r}) \cdot \Phi_{lm}^{(i)*}(\mathbf{r}) dV$ denotes the projection coefficients.

The *l*-th orbital of the β -species contributes to the population by a fraction of $h_{nk,l}^{(\beta)}$ ⁴⁵⁾

$$h_{nk,l}^{(\beta)} = \frac{\sum_{i \in (\beta)} \sum_{m=-l}^{m=+l} C_{nk,lm}^{(i)} C_{nk,lm}^{(i)^*}}{\sum_{i \in (\beta,\beta,\gamma,\dots)} \sum_{l} \sum_{m=-l}^{m=+l} C_{nk,lm}^{(i)} C_{nk,lm}^{(i)^*}}.$$
 (6)

By using the planewave basis set in the PPP scheme, the representation of natural atomic orbitals around the centers of atoms is missing. However, this disadvantage could be overcome by projecting the Bloch states onto the atomic orbitals constructed using the radial pseudoatomic wave functions of each angular momentum channel for each element (the angular parts are simply spherical harmonic functions). 46,47) It is useful for extracting the local (atomic) information of the materials. The radial pseudoatomic wave functions are those used to generate pseudopotentials and therefore, had the best consistency with the Bloch states. The projected values are equivalent to the coefficients of LCAO-type expansion of original Bloch states using pseudoatomic orbitals as basis functions. Taken together, these coefficients can be used to extract local information from the system as a whole, where in the present work it is the partial or projected density of states (PDOS) plots that are used as an analysis tool. This atomic projection concept is then employed for resolving interesting components from the total density of states (TDOS)

$$PDOS(\beta, l, E) = \sum_{n} \sum_{k} h_{nk,l}^{(\beta)} \delta(E - E_{nk})$$
 (7)

PDOS could be used to provide valuable insight into the formation of energy band gap and the nature of transitions from which the linear and nonlinear optical properties originate.

2.2.3 Optical properties

In a crystalline solid, the most important optical transitions did not change the momentum or the spin of the electrons involved in the transition. In terms of an energy band structure, this means that one only has to consider optical excitations from an occupied state of the same spin for each k vector in BZ.

The linear optical properties of a dielectric crystalline material can therefore be described with a dielectric function of $\epsilon_{ij}(\boldsymbol{q},\omega)$ at $\boldsymbol{q}=0$. When the incident photon energy is higher than the band gap $E_{\rm G}$, the material can attenuate photon flux. The absorption coefficient $\alpha_{ij}(\omega)$ is related to the imaginary part of dielectric function by 48)

$$\operatorname{Im} \epsilon_{ij}(\omega) = \frac{\lambda n(\omega)}{2\pi} \alpha_{ij}(\omega)$$

$$= \frac{8\pi^2 \hbar^2 e^2}{m^2 V} \sum_{k} \sum_{cv} (f_c - f_v)$$

$$\times \frac{p_{cv}^i(k) p_{cv}^j(k)}{E_{vc}^2} \delta[E_{cv}(k) - \hbar \omega]. \tag{8}$$

Here, f_c and f_v reperesented the Fermi distribution of the conduction band c and the valence band v, respectively; p_{cv}^i $(k, \ \mathring{A}^{-1})$ denotes the momentum matrix element (MME, in unit of \mathring{A}^{-1}) from the conduction band c to the valence band v at the k point of BZ. The real part of the dielectric function is obtained from the imaginary part with the Kramer–Kronig transformation. For the second-order nonlinear optical (NLO) response, the theoretical description is very complex. However, at zero frequency limits, NLO susceptibility can be expressed as

$$\chi_{ijk}^{(2)}(0) = \frac{1}{V} \left(\frac{e\hbar}{m}\right)^{3}$$

$$\times \sum_{k} \sum_{vc} \left[\sum_{c'} \frac{1}{E_{c'c}E_{cv}^{2}E_{c'v}^{2}} (D_{vc'c}^{ijk} + D_{cvc'}^{ijk} + D_{c'cv}^{ijk}) - \sum_{v'} \frac{1}{E_{vv'}E_{cv}^{2}E_{c'v}^{2}} (D_{v'cv}^{ijk} + D_{vv'c}^{ijk} + D_{cvv'}^{ijk}) \right], \qquad (9)$$

where $D_{nml}^{ijk} = \text{Im}[p_{nm}^i(p_{ml}^j p_{ln}^k + p_{ml}^k p_{ln}^j)]/2$. Decomposing $\chi_{ijk}^2(0)$ into various contributions from atomic species or orbitals are of interest here. This can be properly carried out by calculating the contribution from the β -th species as⁴⁹⁾

$$\chi_{ijk}^{(2)}(\beta, E) = \frac{1}{V} \left(\frac{e\hbar}{m}\right)^{3} \sum_{l} \sum_{k} \sum_{vc} [h_{vk,l}^{(\beta)} \delta(E - E_{vk}) + h_{ck,l}^{(\beta)} \delta(E - E_{ck})] \times \left(\sum_{c'} \frac{D_{vc'c}^{ijk} + D_{cvc'}^{ijk} + D_{c'cv}^{ijk}}{E_{c'c} E_{c'v}^{2} E_{c'v}^{2}} - \sum_{l} \frac{D_{v'cv}^{ijk} + D_{vv'c}^{ijk} + D_{cvv'}^{ijk}}{E_{vv'} E_{cvv}^{2} E_{c'v}^{2}}\right).$$
(10)

Equation (10) is very similar to eq. (7) except that secondorder nonlinear optical strengths served as the weighting factor. We shall use this equation to obtain insight into the mechanism underlying NLO susceptibility. In §4 the calculated and the experimental results will be compared and discussed.

Tang *et al.* used the same approach in both LDA and generalized-gradient approximation (GGA) with norm-conserving pseudopotentials to investigate the electronic structures, and optical and bulk properties of rhombohedral ternary halides⁶⁾ and orthorhombic ternary nitrides.⁵⁰⁾ The analyses using band-by-band and atomic species projection techniques^{6,50)} both yielded useful information about material properties and provided deep insight into the fundamental understanding of the electronic structures and optical properties of rhombohedral nonlinear optical crystals, $CsGeX_3$ (X = Cl, Br, and I).

2.3 Discussion

The optimized cell parameters obtained by first-principles calculations are compared with the experimental data. The equilibrium lattice constants and fractional atomic coordinates are deduced from total-energy minimization. Relaxation of lattice parameters and atomic positions is carried out under the constraint of the unit cell space-group symmetry. In Table II, CsGeX₃ is crystallized in the noncentrosymmetric rhombohedral space group *R3m*.

The magnitudes of experimental distortional factors in Table II can be simplified as integer ratios. The experimental lattice angles of CGX crystals have the ratio $\Delta\alpha_{\rm exp}^{\rm CGC}:\Delta\alpha_{\rm exp}^{\rm CGB}:\Delta\alpha_{\rm exp}^{\rm CGI}\approx 3:14:16,$ and the first-principles calculation results are $\Delta\alpha_{\rm cal}^{\rm CGC}:\Delta\alpha_{\rm cal}^{\rm CGB}:\Delta\alpha_{\rm cal}^{\rm CGI}\approx 1:2:3.$ Additionally, the experimental values for B-site cation displacement are $d_{\rm Ge,exp}^{\rm CGC}:d_{\rm Ge,exp}^{\rm CGB}:d_{\rm Ge,exp}^{\rm CGI}\approx 3:4:5,$ and the first-principles calculation results are $d_{\rm Ge,cal}^{\rm CGG}:d_{\rm Ge,cal}^{\rm CGI}:d_{\rm Ge,cal}^{\rm CGI}\approx 4:6:7.$ Finally, the experimental values for anion displacement obey the ratio $d_{\rm X,exp}^{\rm CGC}:d_{\rm X,exp}^{\rm CGB}:d_{\rm X,exp}^{\rm CGI}\approx 4:2:1,$ and the first-principles calculation results are the same. The effects of these integer ratios on the

electronic and optical properties will be discussed in the following sections.

3. Electronic and Linear Optical Properties

The first-principles calculations of dielectric function and electronic band structures of rhombohedral nonlinear optical crystals, $CsGeX_3$ (X=Cl, Br, and I), are performed. The maximum difference between calculated and measured lattice parameters are less than 1.1%. However, the optimized lattice angles of $CsGeX_3$ are more distorted from the cubic structure than the reported experimental results (see Table II).

3.1 Electronic band structures and density of states analysis

The CGX crystals rhombohedrally extended along one of the diagonal direction, e.g., [111]. The calculated electronic band structures of rhombohedral CGX crystals behave similarly. As shown in the first row of Fig. 2, CGX has a direct band gap, $E_G = \Delta E_R$, at the R(111)-point. According to the electronic band structures of CGX, as shown in the first row of Fig. 2, band transition energies at Γ -point, ΔE_Γ , are also larger than that at M-point, ΔE_M . In brief, we have $\Delta E_\Gamma > \Delta E_R > \Delta E_R = E_G$ in rhombohedral CGX crystals.

The experimental and calculated band gaps, $E_{\rm G} = \Delta E_{\rm R}$, of CGX decrease from CGC to CGI, as listed in the first two rows in Table III. These electronic band structures of rhombohedral halides have a quite different behavior from those of perovskite oxides, ABO₃, e.g., BaTiO₃, PbTiO₃, SrTiO₃, and LiNbO₃.

As shown in Table III, all the calculated band gaps of rhombohedral CGX crystals are underestimated with respect to the measured values. This is the common problem of LDA approximation. The difference can be remedied if one calculates the GW correction to self-energies. From the results of the density of states analysis shown in the second row of Fig. 2, it is found that cation Ge, which is located on the longest diagonal axis [111], plays a key role in band transition. According to our calculations, there are more than 90% contribution from the p-orbitals of Ge near both the valence-band maximum (VBM) and the conduction-band minimum (CBM) for all CGX crystals. On other hand, the contribution of Cs is smaller than 1% near the band gaps. The anion X provides the remaining contribution near the band gaps.

3.2 Dielectric functions and the structural effects

In Fig. 3, the imaginary and real parts of the dielectric function, $\epsilon''(\omega)$ and $\epsilon'(\omega)$, for CsGeX₃ are presented in the last two rows. In the evaluation of all the response functions, the essential task is the integration of a function over IBZ. This is carried out by a "hybrid" random sampling-tetrahedron method. We partition IBZ into many small tetrahedra, at whose vertices we evaluate the eigenvalues and velocity matrix elements on the basis of results from the calculations. The first peak is associated with $\Delta E_{\rm R} = E_{\rm G}$ optical transition. The second structure in the function for the most part arises from $\Delta E_{\rm M}$ resonance.

According to eq. (8), the dielectric constant at zero frequency of CGX increases from 4.8598 (ϵ'_{CGC}) to 6.5313 (ϵ'_{CGI}). This tendency is attributed to the structural distortion.

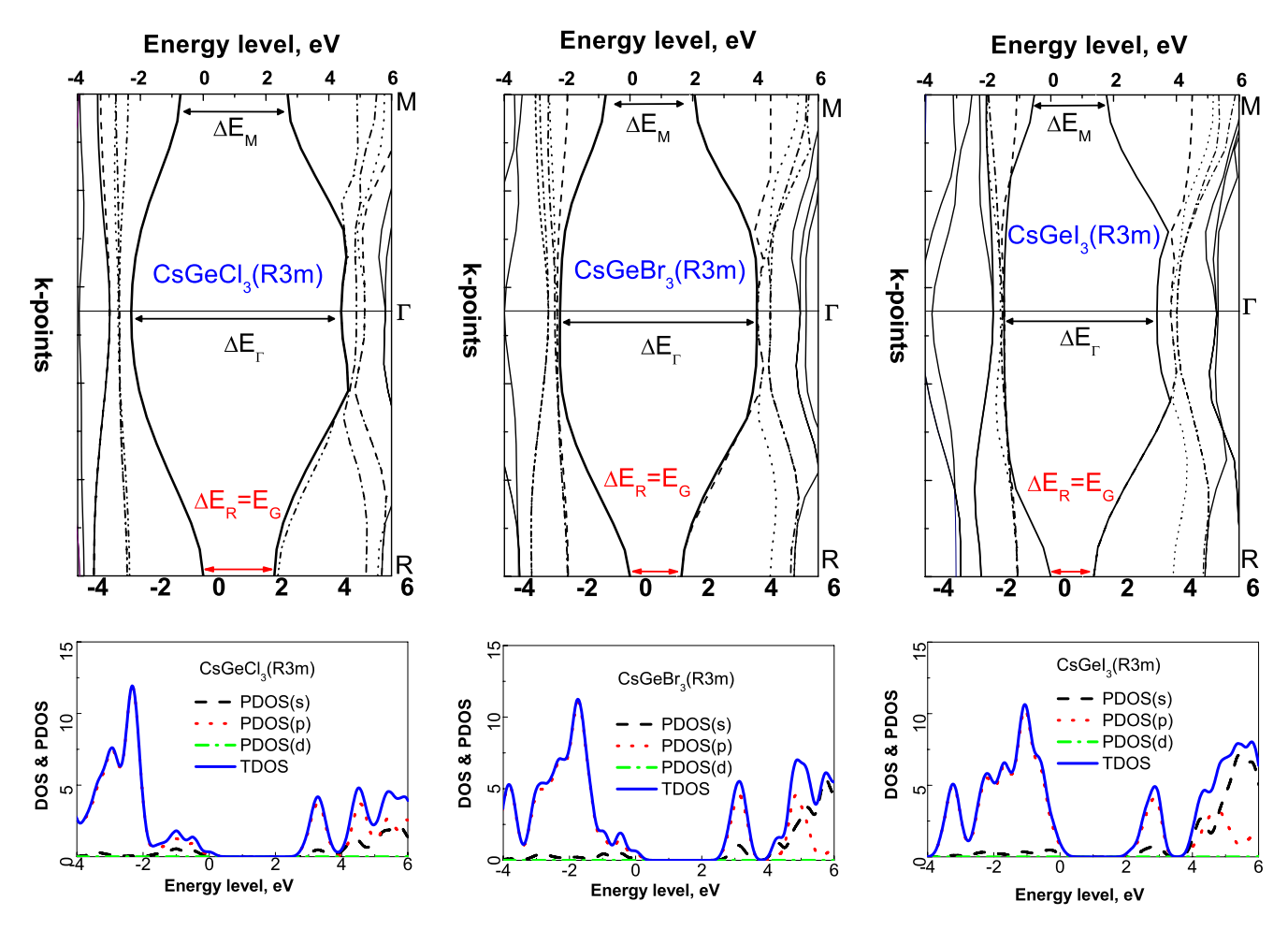


Fig. 2. (Color online) Calculated electronic band structures, and partial densities of state (PDOSs) of rhombohedral CsGeX₃. Partial densities of states (PDOSs) of CsGeX₃ projected onto all species at various atomic orbitals.

Table III. Calculated optical properties, the linear and second-order optical responses, in CsGeX₃ at zero frequency. Nonlinear optical coefficients of NLO crystals CsGeX₃ (X = Cl, Br, and I). They are compared with some available experimental data. The contribution of each species is projected to $\chi^{(2)}_{xzx}$, $\chi^{(2)}_{yyy}$, $\chi^{(2)}_{zzxx}$, and $\chi^{(2)}_{zzzz}$ in rhombohedral CsGeX₃.

NLO crystal	CsGeCl ₃	CsGeBr ₃	CsGeI ₃	
$E_{\rm g,exp}$	3.67	2.32	1.53	
$E_{ m g,cal}$	2.26	1.49	1.02	Direct, R-point
ϵ'	4.8598	5.2521	6.5313	Unpolarized, zero frequency
ϵ'	4.8624	5.2527	6.5331	Unpolarized, Sum rule
ϵ_{zz}'	8.8477	10.183	12.551	Zero-frequency
ϵ'_{xx}	6.6550	7.5837	9.5421	Zero-frequency
$d_{\rm eff,exp}^{(2)}$	2.12	3.46	NA	(pm/V)
$\chi^{(2)}_{zzz}$	11.64924	22.39020	127.7794	Zero-frequency (pm/V)
$\chi_{yyy}^{(2)}$	7.706676	7.041843	33.39160	Zero-frequency (pm/V)
$\chi^{(2)}_{zxx}$	2.629566	2.672494	4.590949	Zero-frequency (pm/V)
$\chi_{xzx}^{(2)}$	2.629567	2.672494	4.590949	Zero-frequency (pm/V)

The dielectric constants are about $\epsilon'_{\rm CGC}:\epsilon'_{\rm CGB}:\epsilon'_{\rm CGI}\approx 12:13:16$, and the first-principles calculated results increases as $d^{\rm CGC}_{\rm Ge,cal}:d^{\rm CGB}_{\rm Ge,cal}:d^{\rm CGI}_{\rm Ge,cal}\approx 4:6:7$ and $\Delta\alpha^{\rm CGC}_{\rm cal}:\Delta\alpha^{\rm CGB}_{\rm cal}\approx 1:2:3$.

4. Nonlinear Optical Properties

Various representative calculations of bulk nonlinear

susceptibilities are discussed in the review paper of Champagne and Bishop.⁵³⁾ In this study, we focused on the structural and the constituent effects on NLO susceptibility, and band-gap correction was not implemented.

CsGeX₃ crystals belong to crystal class 3m, which has the nonvanishing tensor elements, xzx = yzy, xxz = yyz, zxx = zyy, zzz, $yyy = -yxx = -xxy = -xyx^{12-14}$) assuming that Kleinman symmetry is valid.⁵⁴⁾ For comparison, the calculated second-order nonlinear optical susceptibilities at zero frequency, $\chi_{ijk}^{(2)}$, of rhombohedral CGX crystals are shown in Table III.

4.1 Structural effects on second-order nonlinear susceptibilities

At zero frequency limits, NLO susceptibility can be given by eq. (9). Since the photon energy $\hbar\omega$ of PSHG measurement is well below the band gap, the frequency-dependent $\chi^{(2)}_{ijk}(\omega)$ and the refractive index $n(\omega)$ are nearly constant in this frequency region. (13,55) The static $\chi^{(2)}_{ijk}(0)$ can be considered as a good approximation of the frequency-dependent $\chi^{(2)}_{ijk}(-2\omega;\omega,\omega)$ in the PSHG measurements. The integration of the second harmonic pattern over scattering angle yields the total second-harmonic intensity $I_{2\omega}$. The square of the effective nonlinearity $\langle (d^{(2)}_{\rm eff})^2 \rangle$ averaged over the orientation distribution in crystalline powders of CsGeBr₃ is determined by

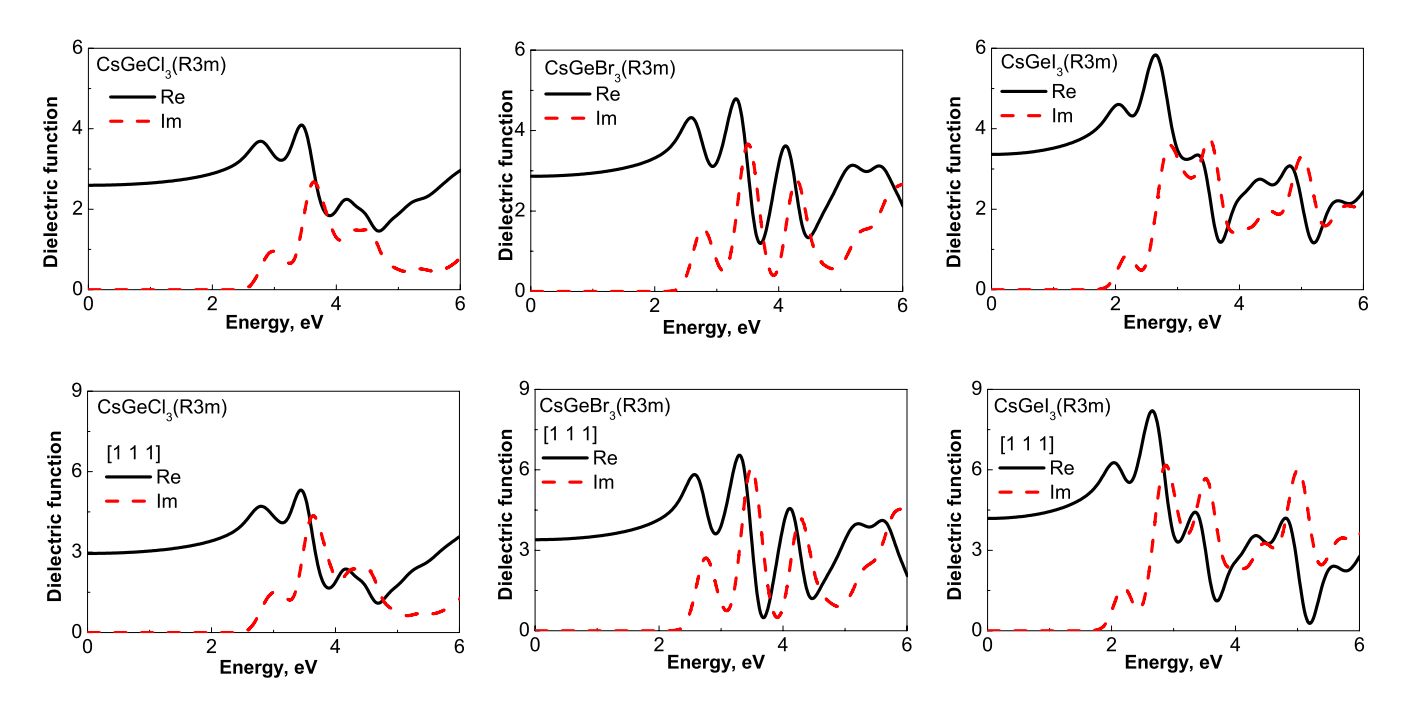


Fig. 3. (Color online) Results for the calculated unpolarized dielectric function (the first row) and dielectric function in [111] direction of rhombohedral CsGeX₃.

$$\langle (d_{\text{eff}}^{(2)})^2 \rangle_{\text{CGB}} = \langle (d_{\text{eff}}^{(2)})^2 \rangle_{\text{KDP}} \cdot \frac{I_{2\omega,\text{CGB}}^{\text{total}} \cdot n_{\omega,\text{CGB}}^2 \cdot n_{2\omega,\text{CGB}}}{I_{2\omega,\text{KDP}}^{\text{total}} \cdot n_{\omega,\text{KDP}}^2 \cdot n_{2\omega,\text{KDP}}}$$

$$\approx \langle (d_{\text{eff}}^{(2)})^2 \rangle_{\text{KDP}} \cdot \frac{I_{2\omega,\text{CGB}}^{\text{total}} \cdot n_{\omega,\text{KDP}}^3}{I_{2\omega,\text{KDP}}^{\text{total}} \cdot n_{\text{KDP}}^3}$$

$$(11)$$

with a reference NLO crystal (e.g., KDP) for $n \approx n_{\omega} \approx n_{2\omega}$. Powder SHG measurements revealed that the SHG efficiencies of CGB are higher than those of CGC. The detected SHG signals were estimated from the reflection signals at various particle sizes, and they showed that the SHG responses of sieved polycrystalline CsGeBr₃ are about 1.62 times larger than those of CsGeCl₃ and 9.63 times larger than those of KDP (see Table III).

 $d_{\rm eff}^{(2)}$ measured by PSHG method, is the accumulated effect, and the PSHG method serves as a screening technique of choosing appropriate NLO materials. It is difficult to simulate second-order NLO tensors, $d_{ijk}^{(2)}$ or $\chi_{ijk}^{(2)}$, from powder measurement. However, the trends of $d_{ijk}^{(2)}$, and $\chi_{ijk}^{(2)}$ should be similar. Besides, there is a semiempirical rule: $d_{\rm eff}^{(2)} \approx d_{ijk}^{(2)} = 1/2\chi_{ijk}^{(2)}$. The calculated with the semiempirical formula of the semiempirical rule: $d_{\rm eff}^{(2)} \approx d_{ijk}^{(2)} = 1/2\chi_{ijk}^{(2)}$.

The calculated nonlinear coefficients of rhombohedral nonlinear optical crystals, CsGeX₃ (X = Cl, Br, and I), are listed in Table III. The nonlinear coefficients of rhombohedral nonlinear optical crystals, CsGeX₃, are compared with the available powder second-harmonic generation (PSHG) measurements. In Table III, $\chi_{ijk}^{(2)}(0)$ obeys the same trends as the magnitudes of dielectric constant of CGX, i.e., $\chi_{CGC}^{(2)}(0) < \chi_{CGB}^{(2)}(0) < \chi_{CGI}^{(2)}(0)$. This trend is also related to that of distortional factors: $d_{Ge}^{CGC} < d_{Ge}^{CGB} < d_{Ge}^{CGI}$.

In general, the magnitude of $\chi_{ijk}^{(2)}$ is about twice that of $d_{eff}^{(2)}$.

In general, the magnitude of $\chi_{ijk}^{(2)}$ is about twice that of $d_{\text{eff}}^{(2)}$. The calculated $\chi_{zzz}^{(2)}$ of CGB is approximately 2.0 times larger than that of CGC crystals and approximately 5.8 times smaller than that of CGI crystals. The reflected SHG signals and the underestimated $d_{\text{eff}}^{(2)}$ of CGB use about 1.63 times larger than those of CsGeCl₃.

4.2 Results and discussion

The species projected contributions to $\chi^{(2)}_{xzx}$, $\chi^{(2)}_{xzx}$, $\chi^{(2)}_{xzx}$, and $\chi^{(2)}_{xzx}$ in rhombohedral CsGeX₃ are shown in Figs. 4, 5, and 6. The main peaks of projected $\chi^{(2)}_{ijk}$ of CGX are observed around the band edges. The dominant contributions come from the species Ge and X. This behavior is similar to that of the dielectric function. The magnitudes of $\chi^{(2)}_{ijk}$ are inversely proportional to the band gaps (shown in the first two rows in Table III), $E^{\text{CGC}}_{\text{G}} > E^{\text{CGB}}_{\text{G}} > E^{\text{CGI}}_{\text{G}}$, of CGX, and are proportional to the degree of distortion.

There are two groups of significant peaks found in each second-order nolinear optical susceptibily. The first group of significant peaks is due to the second term in eq. (10), which is the sum of transitions from all valence states to the components in a conduction-band state associated with a given species, as mediated by all possible intermediate states. Thus, these peaks are related to the conduction-band PDOS. The other group of peaks is due to the first term in eq. (10), which is the sum of transitions from the components in a valence-band state associated with a given species to all valence states, as mediated by all possible intermediate states. Thus, these peaks are related to the valence-band PDOS. We found a close relationship between the relative positions of these peaks and the B-site cation displacement d_{Ge} according to our analysis of B-site cation displacement discussed above, we obtain $d_{
m Ge,cal}^{
m CGC}:d_{
m Ge,cal}^{
m CGB}:d_{
m Ge,cal}^{
m CGI} pprox$ 4:6:7. The magnitudes and energy levels of the strongest peaks in group two are found to be $31.72 \,\mathrm{pm/V}$ at $-0.75 \,\mathrm{eV}$ for CGC, 00, $-46.73 \, pm/V$ at $-1.15 \, eV$ for CGB, and $-93.86 \,\mathrm{pm/V}$ at $-1.35 \,\mathrm{eV}$ for CGI, respectively. The energy levels of the peak deviation $p_{\rm D}$ are in a similar ratio, i.e., $p_{\rm D}^{\rm CGC}:p_{\rm D}^{\rm CGB}:p_{\rm D}^{\rm CGI}\approx 4:6:7.$

There are some reasons for the significant SHG signals of rhombohedral CsGeX₃ crystals. First of all, the SHG responses are contributed by the structural distortion and

4

Tot

Br

Cs

- Ge

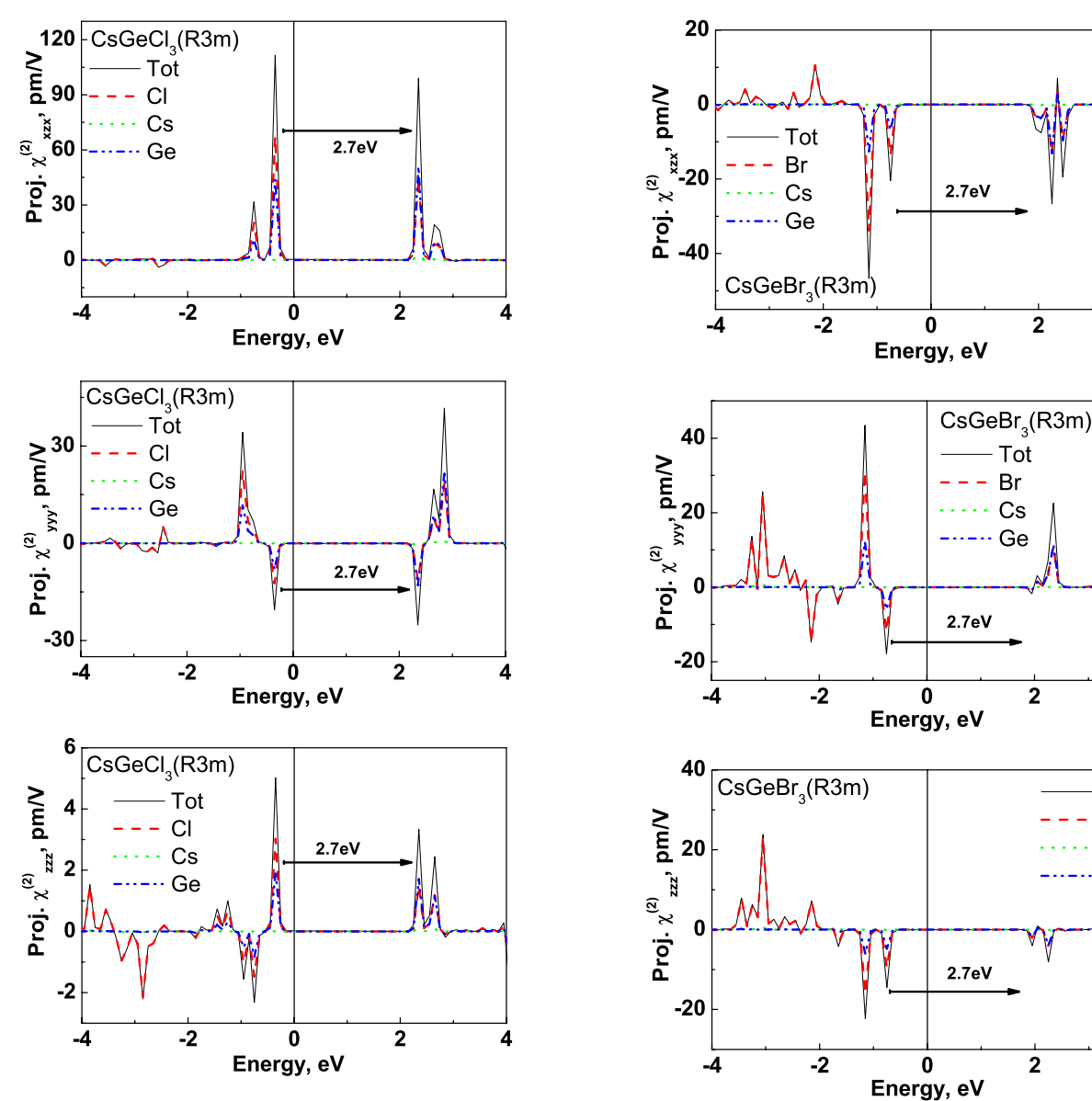


Fig. 4. (Color online) Second-order nonlinear optical susceptibility components of rhombohedral CsGeCl₃ projected for various atomic species and energy bands using eq. (10). The contribution of each species is projected to $\chi^{(2)}_{xzx}$ (= $\chi^{(2)}_{xzx}$), $\chi^{(2)}_{yyy}$, and $\chi^{(2)}_{zzz}$ in CsGeCl₃. Absolute value of SHG susceptibility $\chi^{(2)}_{xyz}(\omega;\omega,0)$, solid line for CsGeCl₃.

Fig. 5. (Color online) Second-order nonlinear optical susceptibility components of rhombohedral CsGeBr₃ projected for various atomic species and energy bands using eq. (10). The contribution of each species is projected to $\chi^{(2)}_{xzx}$ (= $\chi^{(2)}_{xzx}$), $\chi^{(2)}_{yyy}$, and $\chi^{(2)}_{zzz}$ in CsGeBr₃. Absolute value of SHG susceptibility $\chi^{(2)}_{xyz}(\omega;\omega,0)$, solid line for CsGeBr₃.

the off-centered Ge ion in the unit cell. The cell angle distortion of CGB is larger than that of CGC. The position of the B-site cation, Ge in CGB, is closer to the cell corner than that of CGC. $\chi^{(2)}_{zzz}$ increases as these distortions increase. Secondly, the band gap decreases $^{(2)-33}$ and NLO susceptibility increases when the atomic weights of halides increase. $\chi^{(2)}_{ijk}$ is approximately inversely proportional to the cubic of band gap $^{(2)}$ [see eq. (9)]. For the third contribution, it has also been suggested that the electron lone pair, the unbonding electron pair, of Ge that is polarized in the [111] direction could give a stronger MME for incident light polarized along [111]. This explains why the dielectric function for [111] polarized light is stronger than that for unpolarized light, as observed in Fig. 3. The lone pair polarization is also mentioned in previous reports. $^{(29-33)}$ From the spicies-projected scheme, the energy difference is $2.7 \, \text{eV}$, which is contributed by the electron lone pair of

Ge and is identical in the compounds CGC, CGB, and CGI (Figs. 4, 5, and 6). These reasons could be the basis for the important guidelines for further improvement of the NLO crystal design.

Experimental data at energies above the gap are very scarce for the materials considered here. The only data are listed in Table III. The calculated energy band gaps are about 30% smaller than the experimental values; however, this is to be expected at the level of the LDA methodology. The smaller band gap also overestimates NLO susceptibility. Although the smaller band gap obtained with LDA can be corrected with a simple scissors approximation or a more sophisticated GW correction, we did not intend to do so in this study. Our calculated second-order susceptibilities agreed reasonably well with available calculated and experimental results.

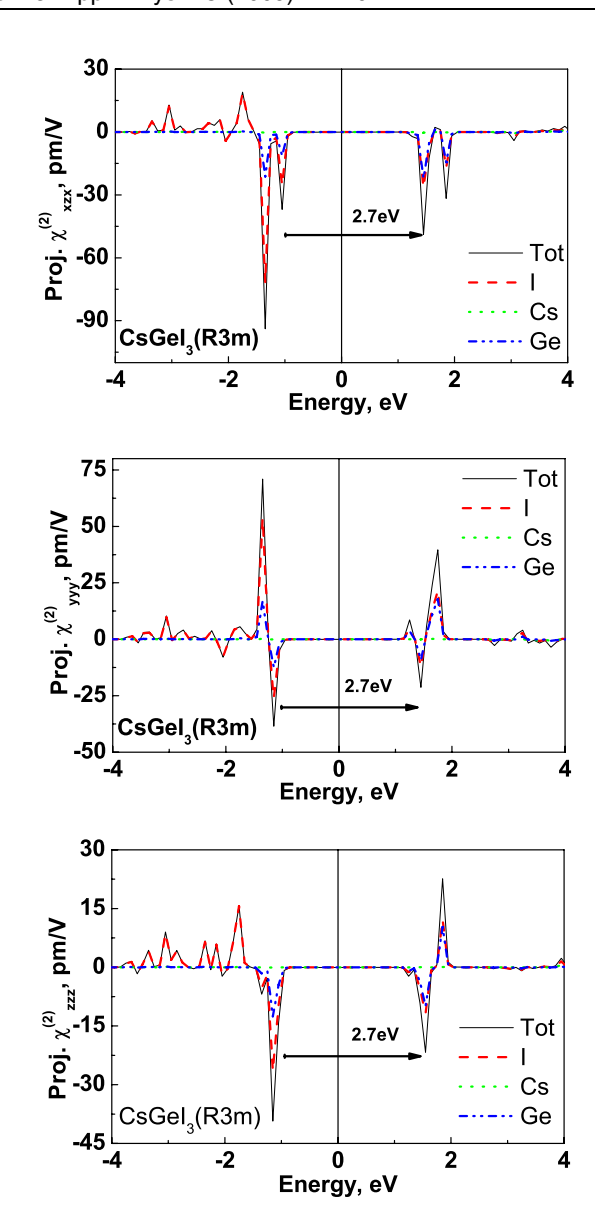


Fig. 6. (Color online) Second-order nonlinear optical susceptibility of components of rhombohedral CsGel $_3$ projected for various atomic species and energy bands using eq. (10). The contribution of each species is projected to $\chi^{(2)}_{xzx}$ (= $\chi^{(2)}_{zzx}$), $\chi^{(2)}_{yyy}$, and $\chi^{(2)}_{zzz}$ in CsGel $_3$. Absolute value of SHG susceptibility $\chi^{(2)}_{xyz}(\omega;\omega,0)$, solid line for CsGel $_3$.

5. Conclusions

The direct effects of structural distortion and electronic properties for linear and second-order optical responses in CsGeX₃ based on first-principles electronic structure calculations are presented. A response formalism that is free of any nonphysical divergences are employed at zero frequency, we obtain calculated results that reasonably agree with experimental results for $\chi^{(2)}_{xyz}(\omega;\omega,0)$ in the low-frequency regime. SHG susceptibility has been presented and it shows important differences from other theoretical calculations. The lack of experimental data, as well as its contradictory nature, prevents any conclusive comparison with experimental results over a large energy range. The structural deformed factors $\Delta \alpha$, d_{Ge} , and d_X are proposed to describe the degree of the distortion from an ideal perovskite structure. $\Delta \alpha$ and d_{Ge} increase while d_X decrease when the halide anions are changed from Cl (3.67 eV) to I (1.5 eV).

The direct structural distortion effect on these rhombohedral CGXs are analyzed via the first-principles calculations. The dielectric function and the second-harmonic generation response coefficient behave similarly to $\Delta\alpha$ and $d_{\rm Ge}$. The direct band gaps, $E_{\rm G}$, of CsGeX $_{\rm 3}$ all occur at the R-point, $\Delta E_{\rm R}$. The band gap values of CGX become smaller, i.e., $E_{\rm G}^{\rm CGC}>E_{\rm G}^{\rm CGB}>E_{\rm G}^{\rm CGI}$ as $\Delta\alpha$ and $d_{\rm Ge}$ increase, i.e., $d_{\rm Ge}^{\rm CGC}<d_{\rm Ge}^{\rm CGI}$. Partial density of states (PDOS) analysis reveals that the valence band maximun (VBM) and conduction band minimum (CBM) are mainly from the porbitals of germanium.

Species-projected contributions to $\chi_{ijk}^{(2)}(\beta, E)$ in CGX are affected by both the structural distortion and electronic band structures. The projection technique successfully differentiated the electronic and structural contributions. The magnitudes of $\chi_{ijk}^{(2)}$ are in agreement with some reported experimental results near the band gap. In summary, we found that the lattice distortion parameters play key roles in determining the linear and nonlinear optical responses of CGX crystals.

Acknowledgments

The authors are indebted to the financial support from the National Science Council of the Republic of China under grants NSC 97-2112-M-009-013 and NSC 97-2112-M-032-004-MY2. The authors are also grateful to the National Center for High-Performance Computing for computer time and facilities.

- 1) D. M. Burland: Chem. Rev. 94 (1994) 1.
- Nonlinear Optical Properties of Organic Molecules and Crystals, ed. D. S. Chemla and J. Zyss (Academic Press, Orlando, FL, 1987).
- J. Zhang: Ph. D. thesis, Department of Material Science, Wuhan University (1995).
- M. D. Ewbank, F. Cunningham, R. Borwick, M. J. Rosker, and P. Gunter: CLEO97, 1997, paper CFA7, p. 462.
- J. Zhang, N. Su, C. Yang, J. Qin, N. Ye, B. Wu, and C. Chen: Proc. SPIE 3556 (1998) 1.
- 6) L.-C. Tang, C.-S. Chang, and J. Y. Huang: J. Phys.: Condens. Matter
- 12 (2000) 9129.7) Q. Gu, Q. Pan, W. Shi, X. Sun, and C. Fang: Prog. Cryst. Growth
- Charact. Mater. 40 (2000) 89.

 8) Q. Gu, Q. Pan, X. Wu, W. Shi, and C. Fang: J. Cryst. Growth 212
- 8) Q. Gu, Q. Pan, X. Wu, W. Shi, and C. Fang: J. Cryst. Growth 212 (2000) 605.
- Q. Gu, C. Fang, W. Shi, X. Wu, and Q. Pan: J. Cryst. Growth 225 (2001) 501.
- L. C. Tang, J. Y. Huang, C. S. Chang, M. H. Lee, and L. Q. Liu: J. Phys.: Condens. Matter 17 (2005) 7275.
- 11) P. Ren, J. Qin, and C. Chen: Inorg. Chem. 42 (2003) 8.
- V. G. Dmitriev, G. G. Gurzadyan, and D. N. Nikogosyan: Handbook of Nonlinear Optical Crystals (Springer, Berlin, 1999) 3rd ed.
- 13) R. W. Boyd: Nonlinear Optics (Academic Press, Boston, MA, 2003).
- J. F. Nye: Physical Properties of Crystals (Oxford University Press, Oxford, U.K., 1957).
- V. M. Goldschmidt: Ber. Dtsch. Chem. Ges. 60 (1927) 1263 [in German].
- 16) V. M. Goldschmidt: Fortschr. Min. 15 (1931) 73 [in German].
- 17) J. E. Sipe and E. Ghahramani: Phys. Rev. B 48 (1993) 11705.
- 18) C. Aversa and J. E. Sipe: Phys. Rev. B 52 (1995) 14636.
- 19) A. D. Corso and F. Mauri: Phys. Rev. B 50 (1994) 5756.
- D. J. Moss, J. E. Sipe, and H. M. van Driel: Phys. Rev. B 36 (1987) 1153.
- D. J. Moss, E. Ghahramani, J. E. Sipe, and H. M. van Driel: Phys. Rev. B 41 (1990) 1542.
- E. Ghahramani, D. J. Moss, and J. E. Sipe: Phys. Rev. B 43 (1991) 8990.

- E. Ghahramani, D. J. Moss, and J. E. Sipe: Phys. Rev. B 43 (1991)
- D. J. Moss, E. Ghahramani, and J. E. Sipe: Phys. Status Solidi B 164 (1991) 587.
- 25) M. Z. Huang and W. Y. Ching: Phys. Rev. B 45 (1992) 8738.
- 26) M. Z. Huang and W. Y. Ching: Phys. Rev. B 47 (1993) 9464.
- 27) W. Y. Ching and M. Z. Huang: Phys. Rev. B 47 (1993) 9479.
- 28) Z. H. Levine and D. C. Allan: Phys. Rev. B 44 (1991) 12781.
- U. Schwarz, H. Hillebrecht, M. Kaupp, K. Syassen, H.-G. von Schnering, and G. Thiele: J. Solid State Chem. 118 (1995) 20.
- U. Schwarz, F. Wagner, K. Syassen, and H. Hillebrecht: Phys. Rev. B 53 (1996) 12545.
- G. Thiele, H. W. Rotter, and K. D. Schmidt: Z. Anorg. Allg. Chem. 545 (1987) 148.
- G. Thiele, H. W. Rotter, and K. D. Schmidt: Z. Anorg. Allg. Chem. 559 (1988) 7.
- D.-K. Seo, N. Gupta, M.-H. Whangbo, H. Hillebrecht, and G. Thiele: Inorg. Chem. 37 (1998) 407.
- 34) F. S. Galasso: Perovskites and High T_c Superconductors (Gordon and Breach, New York, 1990).
- 35) V. Butler, C. R. A. Catlow, B. E. F. Fender, and J. H. Harding: Solid State Ionics 8 (1983) 109.
- L. G. Tejuca, J. L. G. Fierro, and J. M. D. Tascon: Adv. Catal. 36 (1989) 385.
- H. Yokokawa, N. Sakai, T. Kawada, and M. Dokiya: Solid State Ionics
 (1992) 43
- 38) N. W. Thomas: Br. Ceram. Trans. 96 (1997) 715.
- 39) R. D. Shannon and C. T. Prewitt: Acta Crystallogr., Sect. B 25 (1969)

- 40) R. D. Shannon: Acta Crystallogr., Sect. A 32 (1976) 751.
- M. C. Payne, M. P. Teter, D. C. Allan, T. A. Arieas, and J. D. Joannopoulos: Rev. Mod. Phys. 64 (1992) 1045.
- 42) H. J. Monkhorst and J. D. Pack: Phys. Rev. B 13 (1976) 5188.
- H. Krakauer, M. Posternak, and A. J. Freeman: Phys. Rev. B 19 (1979) 1706.
- 44) E. Wimmer, H. Krakauer, M. Weinert, and A. J. Freeman: Phys. Rev. B 24 (1981) 864.
- D. Sanchez-Portal, E. Artacho, and J. M. Soler: J. Phys.: Condens. Matter 8 (1996) 3859.
- M. D. Segall, C. J. Pickard, R. Shah, and M. C. Payne: Mol. Phys. 89 (1996) 571.
- 47) M. D. Segall, R. Shah, C. J. Pickard, and M. C. Payne: Phys. Rev. B 54 (1996) 16317.
- S. N. Rashkeev, W. R. L. Lambrecht, and B. Segall: Phys. Rev. B 57 (1998) 3905.
- 49) C. G. Duan, J. Li, Z. Q. Gu, and D. S. Wang: Phys. Rev. B **59** (1999) 369.
- J. Y. Huang, L. C. Tang, and M. H. Lee: J. Phys.: Condens. Matter 13 (2001) 10417.
- 51) M. S. Hybertsen and S. G. Louie: Phys. Rev. B 34 (1986) 5390.
- M. van Schilfgaarde, T. Kotani, and S. Faleevt: Phys. Rev. Lett. 96 (2006) 226402.
- 53) B. Champagne and D. M. Bishop: Adv. Chem. Phys. 126 (2003) 41.
- 54) D. A. Kleinman: Phys. Rev. 126 (1962) 1977.
- W. K. Chen, C. M. Cheng, J. Y. Huang, W. F. Hsieh, and T. Y. Tseng: J. Phys. Chem. Solids 61 (2000) 969.
- 56) Y. R. Shen: The Principles of Nonlinear Optics (Wiley, New York, 2002).